AIAA/AAS Astrodynamics Specialist Conference and Exhibit
21 - 24 August 2006, Keystone, Colorado

AIAA 2006-6178

Solar Sailing Kinetic Energy Impactor (KEI) Mission Design Tradeoffs for Impacting and Deflecting Asteroid 99942 Apophis

Bernd Dachwald* and Ralph Kahle†
German Aerospace Center (DLR), 82234 Wessling, Germany

Bong Wie‡
Arizona State University, Tempe, AZ 85287, USA

Near-Earth asteroid 99942 Apophis provides a typical example for the evolution of asteroid orbits that lead to Earth-impacts after a close Earth-encounter that results in a resonant return. Apophis will have a close Earth-encounter in 2029 with potential very close subsequent Earth-encounters (or even an impact) in 2036 or later, depending on whether it passes through one of several so-called gravitational keyholes during its 2029-encounter. Several pre-2029-deflection scenarios to prevent Apophis from doing this have been investigated so far. Because the keyholes are less than 1 km in size, a pre-2029 kinetic impact is clearly the best option because it requires only a small change in Apophis' orbit to nudge it out of a keyhole. A single solar sail Kinetic Energy Impactor (KEI) spacecraft that impacts Apophis from a retrograde trajectory with a very high relative velocity (75-80 km/s) during one of its perihelion passages at about 0.75 AU would be a feasible option to do this. The spacecraft consists of a 160 m × 160 m, 168 kg solar sail assembly and a 150 kg impactor. Although conventional spacecraft can also achieve the required minimum deflection of 1 km for this approx. 320 m-sized object from a prograde trajectory, our solar sail KEI concept also allows the deflection of larger objects. In this paper, we also show that, even after Apophis has flown through one of the gravitational keyholes in 2029, solar sail Kinetic Energy Impactor (KEI) spacecraft are still a feasible option to prevent Apophis from impacting the Earth, but many KEIs would be required for consecutive impacts to increase the total Earth-miss distance to a safe value. In this paper, we elaborate potential pre- and post-2029 KEI impact scenarios for a launch in 2020, and investigate tradeoffs between different mission parameters.

I. Introduction

Near-Earth objects (NEOs) are asteroids and short-period comets with orbits that intersect or pass near the orbit of Earth (perihelion ≤ 1.3 AU). 838 near-Earth asteroids (NEAs) with an absolute magnitude $H \leq 18$ (diameter $d \gtrsim 1$ km) are currently known (Ref. 1, August 2006), but the entire population contains perhaps more than 1 000 objects of this size (Ref. 2). All NEAs with an Earth Minimum Orbit Intersection Distance (MOID) ≤ 0.05 AU and $H \leq 22$ ($d \gtrsim 200$ m) are termed Potentially Hazardous Asteroids (PHAs). According to the latest discovery statistics at Ref. 1, there are currently 789 known PHAs, 160 of them with $H \leq 18$ ($d \gtrsim 1$ km), and 8 of them with $H \leq 15$ ($d \gtrsim 5$ km). They pose a significant hazard to human civilization and to life on Earth. Today it is widely accepted that NEO impacts have caused at least one mass extinction, 65 million years ago at the Cretaceous/Tertiary boundary, and they are suspected to have caused several global catastrophes before (Refs. 3 and 4). A 2 km object is capable of causing catastrophic

*Scientist, German Space Operations Center, Mission Operations Section, Oberpfaffenhofen, bernd.dachwald@dlr.de, +49-8153-28 2772, Member AIAA, Member AAS.
†Scientist, German Space Operations Center, Space Flight Technology Section, Oberpfaffenhofen, ralph.kahle@dlr.de, +49-8153-28 2451.
‡Professor, Dept. of Mechanical & Aerospace Engineering, bong.wie@asu.edu, +1-480-965 8674, Associate Fellow AIAA.

alteration of the global ecosystem (Ref. 5). Ocean impacts of even smaller objects are of some concern because the destructive potential caused by the resulting tsunamis may be above that from a land impact (Refs. 5 and 6). Even objects that do not intersect Earth's orbit may evolve into Earth-crossers because their orbits are chaotic, having a relatively short dynamical lifetime in the order of $10^7 - 10^8$ years (Refs. 7, 8 and 9).

The use of solar sails to achieve impacts from retrograde orbits was first proposed (and elaborated in a more general way) by McInnes in Refs. 10 and 11. Wie employed in Refs. 12 and 13 the same idea for a fictional asteroid deflection problem by AIAA and made a preliminary conceptual mission design. In Ref. 14, Dachwald and Wie made a more rigorous trajectory optimization study for this fictional AIAA mission scenario. Already in the 1970s, it was first found by Wright in Refs. 15 and 16 and further examined by Sauer in Ref. 17 that the best way to attain a retrograde orbit with a solar sail is to first spiral inwards to a close solar distance and then to use the large available solar radiation pressure to crank the orbit.

The results in Ref. 14 show that solar sail Kinetic Energy Impactor (KEI) spacecraft that impact the asteroid with very high relative velocity from a retrograde trajectory are a realistic option for mitigating the impact threat from near-Earth asteroids (NEAs). In June 2004, the NEA threat scenario became reality. A NEA with a diameter of about 320 m was discovered, which will have a very close encounter with Earth on 13 Apr 2029 and, with a non-negligible probability, subsequent very close encounters or even an impact on 13 Apr 2036, 13 Apr 2037, or later (Refs. 18, 19, and 20). This NEA first got the provisional designation 2004 MN4 and later the designation 99942 Apophis. The currently estimated probability that Apophis impacts the Earth is 1/40 000 for a 2036-encounter and 1/10 638 000 for a 2037-encounter (Ref. 19, August 2006). Note that the current probability of a catastrophic impact in 2036 is higher than, e.g., the probability for an airplane to crash during a flight. Apophis would impact the Earth with a velocity of about 12.6 km/s and the released energy would equal about 875 Megatons of TNT (Ref. 19). Whether or not Apophis will impact the Earth in 2036 or 2037 will be decided by its close encounter in 2029. If the asteroid passes through one of several so-called "gravitational keyholes", it will get into a resonant orbit and impact the Earth in one of its later encounters, if no counter-measures are taken. This paper is about the application of the solar sail KEI concept to remove the real threat from this asteroid.

The classical orbital elements of Apophis in the J2000 heliocentric ecliptic reference frame are (Ref. 18):

$$\begin{aligned} \text{Epoch} &= 53700 \\ a &= 0.92242\,\text{AU} \\ e &= 0.191015 \\ i &= 3.331\,\text{deg} \\ \omega &= 126.364\,\text{deg} \\ \Omega &= 204.466\,\text{deg} \\ M &= 111\,\text{deg} \end{aligned}$$

Apophis' size (H = 19.2) and taxonomic type are not definitely known at this time (Ref. 19). According to Ref. 18, e.g., Apophis has a diameter of $430 - 970$ m. In accordance with Ref. 19, we assume for our calculations that it is a spherical 320 m diameter asteroid with a typical S-class density of 2 720 kg/m^3 and thus an estimated mass of 4.67×10^{10} kg.

II. Asteroid Deflection Using Kinetic Energy Impacts

The simplest approach to deflect a NEO is to impact it with a massive projectile at a high relative velocity. The highest impact velocities can be achieved from a trajectory that is retrograde to the target's orbit, impacting it during one of its perihelion passages. The change in the object's Earth-miss distance due to the impact depends on the time between the KEI's impact and the object's Earth impact, the lead time Δt_{L}, and the velocity change Δv of the asteroid caused by the impactor. In rough terms, the KEI's impact causes an along-track position shift of (see Refs. 20 and 21)

$$\Delta x = 3 \Delta t_{\text{L}} \Delta v \tag{1}$$

Thus a (typical) Δv of 0.25 mm/s provides a Δx of about 24 km in 1 year.

A successful asteroid deflection mission will require accurate modeling and prediction of the velocity change caused by the impactor. The effective impulse imparted to the asteroid will be the sum of the pure

kinetic impulse (linear momentum) of the impactor plus the impulse due to the "thrust" of material being ejected from the impact crater. The last term can be very significant (even dominant), but its magnitude depends strongly upon the density, yield strength, and porosity of the material of which the asteroid is composed, as well as the mass and relative velocity of the impactor. For example, a head-on collision (at a typical relative velocity of $v_{\text{imp}} = 75\,\text{km/s}$) of a 150 kg impactor on a 4.67×10^{10} kg asteroid yields a pure kinetic-impact Δv of approx. 0.24 mm/s. If the asteroid was composed of hard rock, the modeling of crater ejecta impulse from previous studies by Ahrens and Harris in Ref. 21 would predict an additional Δv of 0.25 mm/s, which yields an "enhancement factor" of about $\xi \approx 2$. If the asteroid was composed of soft rock, the previous studies would predict an even larger additional Δv of 0.67 mm/s, which yields $\xi \approx 3.8$. More recent studies by Holsapple in Ref. 22 also indicate $\xi \approx 4$ for a non-porous asteroid, while it might be as low as $\xi \approx 1.16$ for a porous asteroid, like asteroid 25143 Itokawa, the target of the Hayabusa mission (Ref. 23). In any case, those values are associated with a large uncertainty. An accurate modeling and prediction of the ejecta impulse for various asteroid compositions is therefore a critical part of any kinetic-impact approach. To be on the safe side, we assume the worst case, $\xi = 1.16$, which gives

$$\Delta v = \xi \frac{m_{\text{KEI}}}{m_{\text{Apophis}}} v_{\text{imp}} = 3.73 \times 10^{-9} v_{\text{imp}} \tag{2}$$

Another practical concern of any kinetic-impact approach is the risk that the impact could result in the fragmentation of the asteroid, which could substantially increase the damage upon Earth impact (Ref. 24). The energy required to fragment an asteroid critically depends upon its composition and structure. For example, the specific disruption energy for ice is about 9 J/kg (Ref. 25). Hence the disruption energy for a 320 m diameter asteroid composed largely of ice (density 917 kg/m^3, Ref. 26) is approximately 1.4×10^{11} J. Because the kinetic energy of a 150 kg impactor at a typical relative velocity of 75 km/s would be 4.2×10^{11} J, the ice asteroid would likely fragment. If the asteroid was composed largely of silicates, it would have a disruption energy of approximately 9.3×10^{12} J (the specific disruption energy of silicates is about 200 J/kg, Ref. 25), which is much larger than the kinetic energy delivered by the impactor; such an asteroid would likely stay intact. Therefore, further studies are needed to optimize impactor size, relative impact velocity, and the total number of impactors as functions of the asteroid's size and composition, to ensure that the target will not be fragmented.

III. Scenario

To demonstrate the different possibilities that solar sails offer for mitigating the impact threat from NEOs, we assume the following *fictive* scenario:

1. During the very favorable radar and optical observations in 2013 (see Ref. 20), it is found that Apophis is likely to fly through the gravitational 2036-keyhole in its 2029-encounter and thus have a resonant return to hit the Earth in 2036.

2. At 01 Jan 2020, a solar sail KEI that consists of a 160 m × 160 m, 168 kg solar sail assembly and a 150 kg impactor is launched from Earth (inserted with zero hyperbolic excess energy, $C_3 = 0\,\text{km}^2/\text{s}^2$). It has a characteristic acceleration of $a_c = 0.5\,\text{mm/s}^2$. The solar sail film temperature limit is $T_{\text{lim}} = 240°\text{C}$.

3. After having attained a trajectory that is retrograde to Apophis' orbit, the targeting of the asteroid begins. The solar sail KEI is brought onto a collision trajectory, from where it can impact Apophis on 02 Jan 2026 in the case that Apophis is still likely to fly through the keyhole in 2029. Two kinds of collision trajectories are investigated, a trajectory that maximizes v_{imp} and an exactly retrograde orbit (ERO) that encounters Apophis at every perihelion and aphelion passage. For steps 4-6, the former collision trajectory will be assumed.

4. The mission is aborted before the 2029-encounter because it is found that Apophis is not likely anymore to fly through the keyhole. The impact on 02 Jan 2026 is changed into a close flyby. Instead of aborting the mission, however, the solar sail KEI is brought to a trajectory that maximizes the deflection for a post-2029-encounter impact, for the case that this might be necessary. Note that Apophis' post-encounter orbit is not exactly known at that time, but the worst case orbit (leading to a close encounter in 2036) can be estimated with sufficient accuracy.

5. After the close Earth-encounter on 13 Apr 2029 it is found that Apophis really flew through the 2036-keyhole and thus has a resonant return to hit the Earth on 13 Apr 2036.

6. The solar sail KEI impacts the asteroid shortly after the 2029-encounter on 11 Jun 2029.

6b. Alternatively, for comparison, after its launch on 01 Jan 2020, the solar sail KEI is directly sent onto a collision trajectory that maximizes v_{imp} on 11 Jun 2029.

The KEI consists of a 160 m × 160 m, 168 kg solar sail assembly and a 150 kg impactor. Because of its large ΔV-capability, a solar sailcraft with a relatively modest characteristic acceleration of 0.5 mm/s^2 can achieve a trajectory that is retrograde to Apophis' orbit within 4.4 years. After the trajectory is made retrograde to Apophis' orbit, the KEI is brought onto a collision trajectory, so that it impacts Apophis with a large head-on velocity at its perihelion of 0.746 AU (where the impact is most effective). Such a head-on collision yields an impact velocity in the order of $75 - 80$ km/s, which is much larger than the typical impact velocity of about 10 km/s of conventional prograde missions such as NASA's Deep Impact mission (Refs. 27 and 28) or ESA's projected Don Quijote mission (Ref. 29). For the small Apophis target, the impactor is to be separated from the solar sail prior to the impact because of the extremely demanding terminal guidance and targeting requirements. With $v_{\text{imp}} \approx 75$ km/s, each impactor will, depending on Apophis' porosity, cause an estimated Δv of about $0.25 - 1.0$ mm/s in Apophis' trajectory. Figure 1 shows a potential trajectory for a pre-2029-encounter impact.

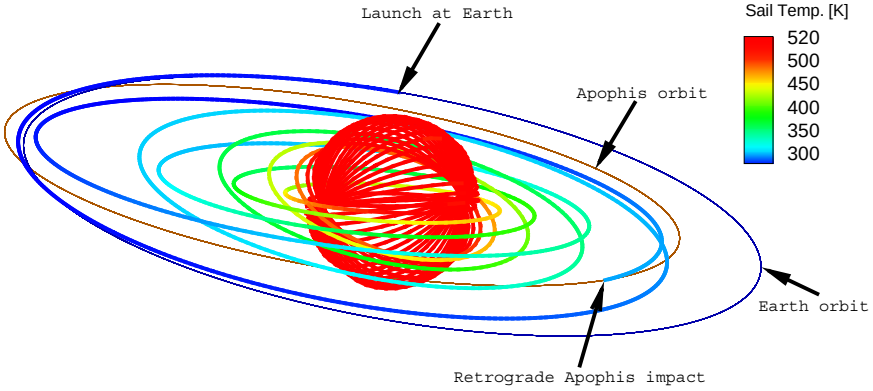

Figure 1. Potential trajectory for a pre-2029-encounter impact

The critical technologies required for the proposed mission include: (1) deployment and control of a 160 m × 160 m solar sail, (2) development of a solar sail and a micro-spacecraft bus that is able to withstand the extreme space environment at less than only 0.25 AU from the sun, (3) autonomous precision navigation, terminal guidance and targeting, and (4) accurate impact-crater ejecta modeling and Δv-prediction. A 160 m × 160 m solar sail is currently not available. However, a 20 m × 20 m solar sail structure was already deployed on ground in a simulated gravity-free environment at DLR in December 1999, a 40 m × 40 m solar sail is being developed by NASA and industries for a possible flight-validation experiment within 10 years, and thus a 160 m × 160 m solar sail is expected to be available within about 15–20 years of a sharply pursued technology development program.

IV. Solar Sail Force Model

For the description of the solar radiation pressure (SRP) force exerted on a solar sail, it is convenient to introduce two unit vectors. The first one is the sail normal vector $\boldsymbol{n}$, which is perpendicular to the sail surface and always directed away from the sun. Let $\mathcal{O} = \{\boldsymbol{e}_r, \boldsymbol{e}_t, \boldsymbol{e}_h\}$ be an orthogonal right-handed coordinate frame, where $\boldsymbol{e}_r$ points always along the sun-spacecraft line, $\boldsymbol{e}_h$ is the orbit plane normal (pointing along the spacecraft's orbital angular momentum vector), and $\boldsymbol{e}_t$ completes the right-handed coordinate system ($\boldsymbol{e}_r \times \boldsymbol{e}_t = \boldsymbol{e}_h$). Then in $\mathcal{O}$, the direction of the sail normal vector, which describes the sail attitude, is expressed by the pitch angle α and the clock angle δ (Fig. 2). The second unit vector is the thrust unit vector $\boldsymbol{m}$, which points along the direction of the SRP force. Its direction is described likewise by the cone angle θ and the clock angle δ.

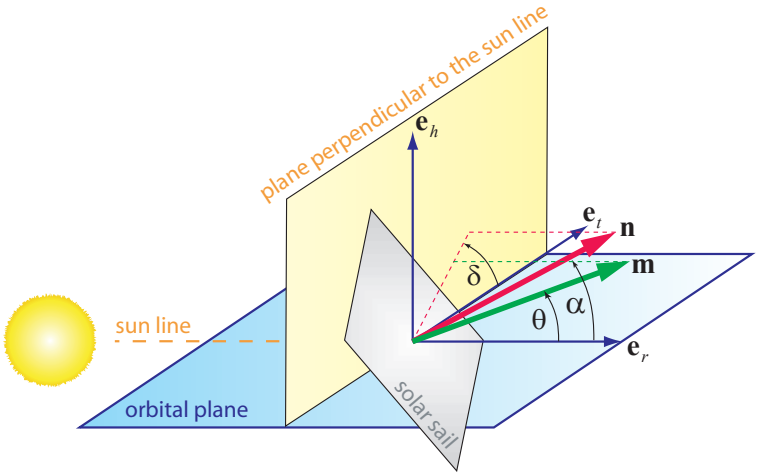

Figure 2. Definition of the sail normal vector and the trust normal vector

At a distance r from the sun, the SRP is

$$P = \frac{S_0}{c}\left(\frac{r_0}{r}\right)^2 = 4.563\,\frac{\mu\mathrm{N}}{\mathrm{m}^2}\cdot\left(\frac{r_0}{r}\right)^2 \tag{3}$$

where $S_0 = 1368\,\mathrm{W/m^2}$ is the solar constant, c is the speed of light in vacuum, and $r_0 = 1\,\mathrm{AU}$.

In this paper, the standard SRP force model for non-perfect reflection from Ref. 30 by Wright is employed, which uses the set of optical coefficients $\mathcal{P} = \{\rho, s, \varepsilon_\mathrm{f}, \varepsilon_\mathrm{b}, B_\mathrm{f}, B_\mathrm{b}\}$ to parameterize the optical characteristics of the sail film, where ρ is the reflection coefficient, s is the specular reflection factor, ε_f and ε_b are the emission coefficients of the front and back side, respectively, and B_f and B_b are the non-Lambertian coefficients of the front and back side, respectively, which describe the angular distribution of the emitted and the diffusely reflected photons. According to Ref. 30, the optical coefficients for a solar sail with a highly reflective aluminum-coated front side and a highly emissive chromium-coated back side (to keep the sail temperature moderate) are $\mathcal{P}_{\mathrm{Al|Cr}} = \{\rho = 0.88, s = 0.94, \varepsilon_\mathrm{f} = 0.05, \varepsilon_\mathrm{b} = 0.55, B_\mathrm{f} = 0.79, B_\mathrm{b} = 0.55\}$. It can be shown (see Ref. 31) that in a sail-fixed 2D coordinate frame $\mathcal{S} = \{\boldsymbol{n}, \boldsymbol{t}\}$ (see Fig. 3; because of symmetry, the third dimension is not relevant here), the SRP force exerted on the solar sail has a normal component $F_\perp$ (along $\boldsymbol{n}$) and a tangential component $F_{||}$ (along $\boldsymbol{t}$) with

$$F_\perp = \boldsymbol{F}_\mathrm{SRP}\cdot\boldsymbol{n} = 2PA\cos\alpha\,\psi_\perp \tag{4a}$$
$$F_{||} = \boldsymbol{F}_\mathrm{SRP}\cdot\boldsymbol{t} = -2PA\cos\alpha\,\psi_{||} \tag{4b}$$

where A is the sail area and

$$\psi_\perp = a_1\cos\alpha + a_2 \tag{5a}$$
$$\psi_{||} = a_3\sin\alpha \tag{5b}$$

with

$$a_1 \triangleq \frac{1}{2}(1+s\rho) \qquad a_2 \triangleq \frac{1}{2}\left[B_\mathrm{f}(1-s)\rho + (1-\rho)\frac{\varepsilon_\mathrm{f}B_\mathrm{f} - \varepsilon_\mathrm{b}B_\mathrm{b}}{\varepsilon_\mathrm{f}+\varepsilon_\mathrm{b}}\right] \qquad a_3 \triangleq \frac{1}{2}(1-s\rho) \tag{6}$$

By defining $\Psi \triangleq (\psi_\perp^2 + \psi_{||}^2)^{1/2}$, the total SRP force vector may then be written as

$$\boldsymbol{F}_\mathrm{SRP} = 2PA\cos\alpha\,\Psi\,\boldsymbol{m} \tag{7}$$

where Ψ depends only on the pitch angle α and the optical coefficients $\mathcal{P}$ of the sail film. The angle between $\boldsymbol{m}$ and $\boldsymbol{n}$, $\phi = \arctan(\psi_{||}/\psi_\perp)$, is called the centerline angle. The cone angle, i.e. the angle between $\boldsymbol{m}$ and the radial unit vector $\boldsymbol{e}_r$, is then $\theta = \alpha - \phi = \alpha - \arctan(\psi_{||}/\psi_\perp)$.

The most commonly used solar sail performance parameter is the characteristic acceleration a_c. It is defined as the SRP acceleration acting on a solar sail that is oriented perpendicular to the sun line ($\boldsymbol{n} \equiv \boldsymbol{e}_r$)

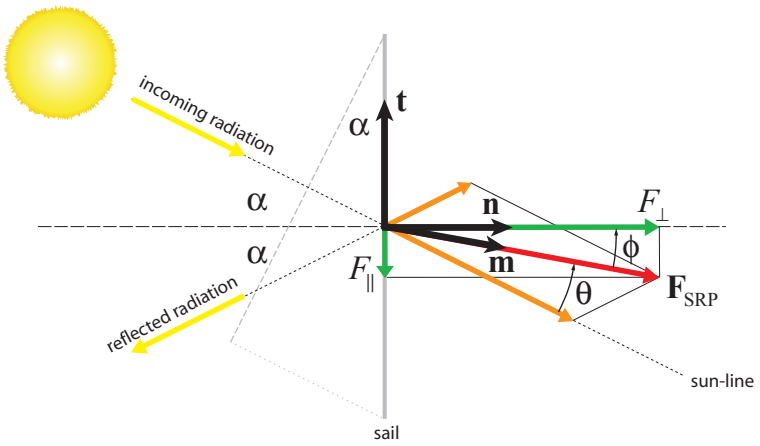

Figure 3. SRP force on a solar sail according to the non-perfectly reflecting force model

at r_0 (1 AU). For the non-perfectly reflecting SRP force model, it is

$$a_c = \frac{2P_0 A}{m}(a_1 + a_2) \tag{8}$$

where $P_0 = P(r = r_0)$ and m is the sailcraft mass.

V. Simulation Model

Besides the gravitational forces of all celestial bodies and the SRP force, many disturbing forces influence the motion of solar sails in space, as they are caused, e.g., by the solar wind, the finiteness of the solar disk, the reflected light from close celestial bodies, and the aberration of solar radiation (Poynting-Robertson effect). Furthermore, a real solar sail bends and wrinkles, depending on the actual solar sail design (Ref. 32). Finally, for a mission that is to target the center of mass of a 320 m-object with a relative velocity of more than 75 km/s, relativistic corrections may have to be applied for the final targeting phase. All these issues have to be considered for high precision trajectory determination and control, as it is required for this mission. For mission feasibility analysis, however, as it is done within this paper, the following simplifications can be made:

1. The solar sail is a flat plate.
2. The solar sail is moving under the sole influence of solar gravitation and radiation.
3. The sun is a point mass and a point light source.
4. The solar sail attitude can be changed instantaneously.

Let the reference frame $\mathcal{I} = \{\boldsymbol{e}_x, \boldsymbol{e}_y, \boldsymbol{e}_z\}$ be a heliocentric inertial right-handed coordinate frame. The equations of motion for a solar sail in the $\mathcal{I}$-frame are:

$$\dot{\boldsymbol{r}} = \boldsymbol{v}, \qquad \dot{\boldsymbol{v}} = -\frac{\mu}{r^3}\,\boldsymbol{r} + \frac{\boldsymbol{F}_{\mathrm{SRP}}}{m} + \boldsymbol{a}_d \tag{9}$$

where $\boldsymbol{r} = (r_x, r_y, r_z)$ is the solar sail position, $\boldsymbol{v} = (v_x, v_y, v_z)$ is the solar sail velocity, μ is the sun's gravitational parameter, and $\boldsymbol{a}_d$ is the disturbing acceleration, which is – according to the simplifications made above – neglected within this paper.

VI. Trajectory Optimization Methods

A. Local Steering Laws

Although local steering laws (LSLs) are not a trajectory optimization method in the narrower sense, they give the locally optimal thrust direction to change some specific osculating orbital element of the spacecraft

with a locally maximum rate. To obtain LSLs, Lagrange's planetary equations in Gauss' form may be used, which describe the rate of change of a body's osculating orbital elements due to some (propulsive and/or disturbing) acceleration. This can best be done in the orbit frame $\mathcal{O} = \{\boldsymbol{e}_r, \boldsymbol{e}_t, \boldsymbol{e}_h\}$. According to Ref. 33, the equations for the semi-major axis a and the inclination i can be written as

$$\frac{da}{dt} = \frac{2a^2}{h}\left(e \sin f a_r + (p/r)\, a_t\right) \tag{10a}$$

$$\frac{di}{dt} = \frac{1}{h} r \cos(\omega + f) a_h \tag{10b}$$

where a_r, a_t, and a_h are the acceleration components along the $\mathcal{O}$-frame unit vectors, $h = |\boldsymbol{h}|$ is the orbital angular momentum per spacecraft unit mass, e is the eccentricity, ω is the argument of perihelion, f is the true anomaly, and p is the semilatus rectum of the orbit. Because Eqs. (10) can be written as

$$\frac{da}{dt} = \frac{2a^2}{h} \begin{pmatrix} e \sin f \\ p/r \\ 0 \end{pmatrix} \cdot \begin{pmatrix} a_r \\ a_t \\ a_h \end{pmatrix} = \boldsymbol{k}_a \cdot \boldsymbol{a} \tag{11a}$$

$$\frac{di}{dt} = \frac{1}{h} \begin{pmatrix} 0 \\ 0 \\ r \cos(\omega + f) \end{pmatrix} \cdot \begin{pmatrix} a_r \\ a_t \\ a_h \end{pmatrix} = \boldsymbol{k}_i \cdot \boldsymbol{a} \tag{11b}$$

it is clear that to decrease the semi-major axis with a maximum rate, the thrust vector has to be along the direction $-\boldsymbol{k}_a$ (local steering law $\mathcal{L}_{a^-}$). To increase the inclination with a maximum rate, the thrust vector has to be along the direction $\boldsymbol{k}_i$ ($\mathcal{L}_{i^+}$). Unlike for other spacecraft, however, where the thrust vector can be directed into any desired direction, the SRP force vector of a solar sail is constrained to lie on a "bubble" that is directed away from the sun. Therefore, when using LSLs, the projection of the SRP force vector onto the respective $\boldsymbol{k}$-vector has to be maximized.

B. Evolutionary Neurocontrol

Within this paper, evolutionary neurocontrol (ENC) is used to calculate near-globally optimal trajectories. This method is based on a combination of artificial neural networks (ANNs) with evolutionary algorithms (EAs). ENC attacks low-thrust trajectory optimization problems from the perspective of artificial intelligence and machine learning. Here, it can only be sketched how this method is used to search for optimal solar sail trajectories. The reader who is interested in the details of the method is referred to Refs. 34, 35, and 36. The problem of searching an optimal solar sail trajectory $\boldsymbol{x}^\star[t] = (\boldsymbol{r}^\star[t], \dot{\boldsymbol{r}}^\star[t])$ – where the symbol "$[t]$" denotes the time history of the preceding variable and the symbol "$\star$" denotes its optimal value – is equivalent to the problem of searching an optimal sail normal vector history $\boldsymbol{n}^\star[t]$, as it is defined by the optimal time history of the so-called direction unit vector $\boldsymbol{d}^\star[t]$, which points along the optimal thrust direction. Within the context of machine learning, a trajectory is regarded as the result of a sail steering strategy S that maps the problem relevant variables (the solar sail state $\boldsymbol{x}$ and the target state $\boldsymbol{x}_\mathrm{T}$) onto the direction unit vector, $\mathsf{S} : \{\boldsymbol{x}, \boldsymbol{x}_\mathrm{T}\} \subset \mathbb{R}^{12} \mapsto \{\boldsymbol{d}\} \subset \mathbb{R}^3$, from which $\boldsymbol{n}$ is calculated. This way, the problem of searching $\boldsymbol{x}^\star[t]$ is equivalent to the problem of searching (or learning) the optimal sail steering strategy $\mathsf{S}^\star$. An ANN may be used as a so-called neurocontroller (NC) to implement solar sail steering strategies. It can be regarded as a parameterized function $\mathsf{N}_{\boldsymbol{\pi}}$ (the network function) that is – for a fixed network topology – completely defined by the internal parameter set $\boldsymbol{\pi}$ of the ANN. Therefore, each $\boldsymbol{\pi}$ defines a sail steering strategy $\mathsf{S}_{\boldsymbol{\pi}}$. The problem of searching $\boldsymbol{x}^\star[t]$ is therefore equivalent to the problem of searching the optimal NC parameter set $\boldsymbol{\pi}^\star$. EAs that work on a population of strings can be used for finding $\boldsymbol{\pi}^\star$ because $\boldsymbol{\pi}$ can be mapped onto a string $\boldsymbol{\xi}$ (also called chromosome or individual). The trajectory optimization problem is solved when the optimal chromosome $\boldsymbol{\xi}^\star$ is found. Figure 4 sketches the subsequent transformation of a chromosome into a solar sail trajectory. An evolutionary neurocontroller (ENC) is a NC that employs an EA for learning (or breeding) $\boldsymbol{\pi}^\star$. ENC was implemented within a low-thrust trajectory optimization program called InTrance, which stands for **In**telligent **Tra**jectory optimization using **n**euro**c**ontroller **e**volution. InTrance is a smart global trajectory optimization method that requires only the target body/state and intervals for the initial conditions (e.g., launch date, hyperbolic excess velocity, etc.) as input to find a near-globally optimal trajectory for the specified problem. It works without an initial guess and does not require the attendance of a trajectory optimization expert.

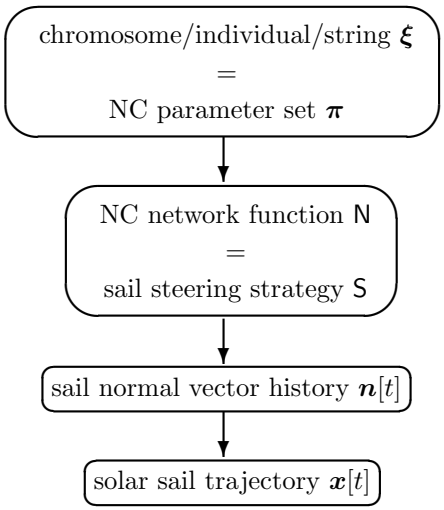

Figure 4. Transformation of a chromosome into a solar sail trajectory

VII. Mission Design

It can be seen from Fig. 1 that the trajectory can be separated into three distinct sub-phases (we use the term"*sub-phase*" because the first two sub-phases will later be combined into one "*phase*"). Generally, orbits with $i < 90\,\text{deg}$ are termed prograde orbits and orbits with $i > 90\,\text{deg}$ are termed retrograde orbits. It was first found by Wright in Refs. 15 and 16 and further examined by Sauer in Ref. 17 that the best way to attain a retrograde orbit with a solar sail is to first spiral inwards to a solar distance that is given by the temperature limit T_{lim} of the solar sail (and the spacecraft), and then to use the large available solar radiation pressure to crank the orbit (although the sail temperature does not only depend on the solar distance but also on the pitch angle, as it will be seen later, Sauer used a minimal solar distance r_{lim} instead of a temperature limit T_{lim}). To simplify the terminology within this paper, we speak of a retrograde orbit (or trajectory), when the orbital angular momentum vector of the spacecraft $\boldsymbol{h}$ and the target $\boldsymbol{h}_{\text{T}}$ are anti-parallel, i.e. $\angle(\boldsymbol{h}, -\boldsymbol{h}_{\text{T}}) = 0\,\text{deg}$. Using LSLs, the strategy to attain such a retrograde orbit divides the trajectory into two well-defined sub-phases

1. Spiralling inwards until the optimum solar distance for cranking the orbit is reached using local steering law $\mathcal{L}_{a^-}$ (the inclination stays constant during this sub-phase)

2. Cranking the orbit until the orbit is retrograde using local steering law $\mathcal{L}_{i^+}$ (the semi-major axis stays nearly constant during this sub-phase). Thereby, it might become necessary to change the ascending node of the orbit, so that the inclination change is $\leq 180\,\text{deg}$.

We regard these two sub-phases as a single phase because, using InTrance, this phase will be optimized in one go. We call this first phase the "orbit-cranking phase". The orbit-cranking phase has to be followed by a second phase (or third sub-phase), for which no simple combination of LSLs exists. We call this second phase the "targeting phase". The goal of the targeting phase is to bring the spacecraft onto a collision trajectory that impacts the target at perihelion with maximum head-on velocity (so the first phase, the orbit-cranking phase, comprises the first sub-phase, the spiralling-in phase, and the second sub-phase, the inclination-raising phase, while the third sub-phase is the second phase, the targeting phase). The time that is spent for the different sub-phases is then $\Delta t = \Delta t_{(a^-)} + \Delta t_{(i^+)} + \Delta t_{\text{trg}} = \Delta t_{\text{oc}} + \Delta t_{\text{trg}}$ with $\Delta t_{\text{oc}} = t_{\text{oc}} - t_0$, and $\Delta t_{\text{trg}} = t_{\text{imp}} - t_{\text{oc}}$. Using InTrance, it was found in Ref. 14 that using LSLs and patching together the solutions of the three sub-phases yields a suboptimal solution because a globally optimal trajectory has a smooth transition between the three sub-phases, changing the inclination also slightly during the first and the third sub-phase, whenever the sailcraft is close to the nodes. Therefore, we define t_{oc}, the end of the orbit-cranking phase, as follows: let $\Delta i_{\measuredangle_{\text{T}}} = |i_{\measuredangle_{\text{T}}} - i|$ be the difference between the inclination i of the spacecraft and the inclination of the retrograde target orbit, $i_{\measuredangle_{\text{T}}} = |180\,\text{deg} - i_{\text{T}}|$. Then $t = t_{\text{oc}}$, when $\Delta i_{\measuredangle_{\text{T}}} = 10\,\text{deg}$.

This means that at the end of the orbit-cranking phase the sailcraft trajectory does not have to be precisely retrograde because this can be accounted for within the targeting phase.

A. Determination of the Optimal Orbit-Cranking Distance

If solar sail degradation is not considered, the acceleration capability of a solar sail increases $\propto 1/r^2$ when going closer to the sun. The minimum solar distance, however, is constrained by the temperature limit of the sail film T_{lim} and the spacecraft (here, however, we consider only the temperature limit of the sail film but not of the spacecraft). The equilibrium temperature of the sail film is (see Ref. 31)

$$T = \left[\frac{S_0}{\sigma} \frac{1-\rho}{\varepsilon_{\mathrm{f}} + \varepsilon_{\mathrm{b}}} \left(\frac{r_0}{r} \right)^2 \cos\alpha \right]^{1/4} \tag{12}$$

where $\sigma = 5.67 \times 10^{-8}\,\mathrm{Wm^{-2}K^{-4}}$ is the Stefan-Boltzmann constant. Thus the sail temperature does not only depend on the solar distance, but also on the sail attitude, $T = T(r, \alpha)$ (and of course on the set of optical parameters $\mathcal{P}$). It was demonstrated in Ref. 37 that faster trajectories can be obtained for a given sail temperature limit T_{lim}, if not a minimum solar distance r_{lim} but T_{lim} is used directly as a constraint. This can be realized by constraining the pitch angle α (that is also the light incidence angle) in a way that it cannot become smaller than the critical pitch angle, where T_{lim} would be exceeded, i.e. $\alpha > \alpha_{\mathrm{lim}}(r, T_{\mathrm{lim}})$.

Although orbit cranking is most effective for a circular orbit, it is also important to consider elliptic orbits. Therefore, we describe the optimal orbit-cranking behavior rather by an orbit-cranking semi-major axis a_{cr} instead of an orbit-cranking radius. Using the direct sail temperature constraint, a_{cr} defines the time $\Delta t_{(i^+)}$ that is required to make the orbit retrograde. $\Delta t_{(i^+)}$ is influenced by two adverse effects, leading to an optimal orbit-cranking semi-major axis $a_{\mathrm{cr,opt}}(T_{\mathrm{lim}})$ where the inclination change rate $\Delta i/\Delta t$ is maximal and thus $\Delta t_{(i^+)}$ is minimal, as it can be seen from Fig. 5. For $a_{\mathrm{cr}} > a_{\mathrm{cr,opt}}$, the inclination change takes longer than for $a_{\mathrm{cr,opt}}$ because of the lower SRP. For $a_{\mathrm{cr}} < a_{\mathrm{cr,opt}}$, the inclination change also takes longer than for $a_{\mathrm{cr,opt}}$ because of the (inefficiently) large critical pitch angle α_{lim} that is required to keep $T < T_{\mathrm{lim}}$. Thus $\Delta t_{(i^+)} = \Delta t_{(i^+)}(T_{\mathrm{lim}})$. It can seen from Fig. 5 that $a_{\mathrm{cr,opt}}(T_{\mathrm{lim}} = 240^\circ\mathrm{C}) = 0.22\,\mathrm{AU}$ where $\Delta i/\Delta t(T_{\mathrm{lim}} = 240^\circ\mathrm{C}, a_c = 0.5\,\mathrm{mm/s^2}) = 0.1642\,\mathrm{deg/day}$.

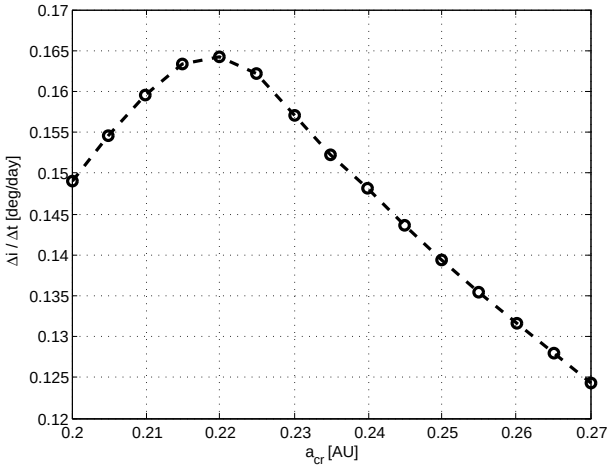

Figure 5. Inclination change rate over orbit-cranking semi-major axis ($T_{\mathrm{lim}} = 240^\circ\mathrm{C}$), circular orbit

B. Trajectory Optimization for the Orbit-Cranking Phase

Knowing that for $T_{\mathrm{lim}} = 240^\circ\mathrm{C}$ the optimal semi-major axis for orbit cranking is 0.22 AU, one might calculate a solar sail trajectory using the local steering laws $\mathcal{L}_{a^-}$ (for the first sub-phase, spiralling-in to $a_{\mathrm{cr,opt}}$) and $\mathcal{L}_{i^+}$ (for the second sub-phase, raising the inclination to $\Delta i_{\curvearrowright_{\mathrm{T}}} = 10\,\mathrm{deg}$). This method, however, yields suboptimal solutions, as previous results found with InTrance have shown (see Ref. 14). Using InTrance, the first two sub-phases are optimized in one go. InTrance yields $\Delta t_{\mathrm{oc}} = 1601\,\mathrm{days}$ for the duration of the orbit-cranking phase (Fig. 6). Figure 6(c) shows a very smooth transition between the two sub-phases. Using

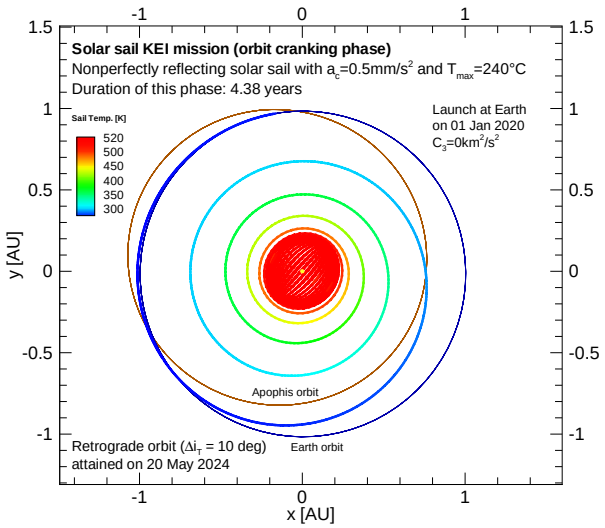

(a) Trajectory for the orbit-cranking phase

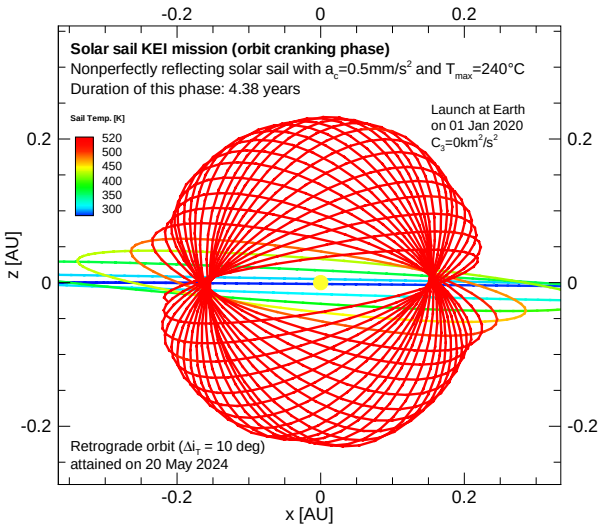

(b) Trajectory for the orbit-cranking phase

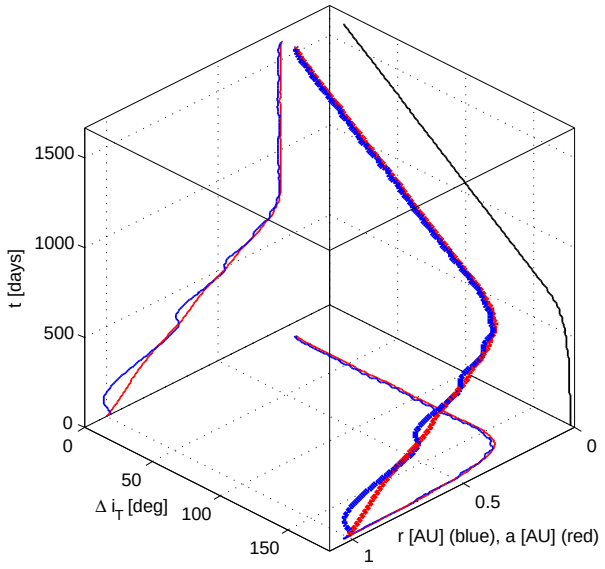

(c) $\Delta i_{\curvearrowright_T}$-$(r,a)$-$t$-diagram

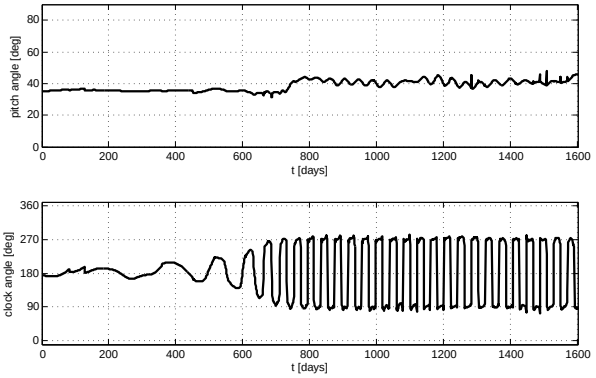

(d) Solar sail control angles

Figure 6. Baseline mission scenario: orbit-cranking phase

LSLs, this transition would be very sharp, as it was shown in Ref. 14. It was also shown in Ref. 14 that the InTrance-solution is about 2.5% faster than a solution that uses LSLs. This is because a global optimal solution changes the inclination also during the first sub-phase (spiralling-in), whenever the solar sail is close to the nodes. Looking at the sail pitch angle in Fig. 6(d), one can see that it is during the inclination-raising phase larger than before, thus avoiding that the sail becomes too hot. Due to the poor *local* search behavior of InTrance, however (note that the control angles are determined by a neural network!), some "noise" remains in the control angles (Fig. 6(d)). Further fine-tuning of the solution with a local trajectory optimization method might therefore yield a marginally faster trajectory.

C. Targeting Trajectory Optimization for the Pre-2029-Encounter

The goal of the targeting phase is to bring the spacecraft onto a collision trajectory that impacts the target at perihelion with maximum head-on velocity. Therefore, the impact date was constrained to be at one of Apophis' perihelion passages and the optimization objective used for InTrance was: maximize $\boldsymbol{v} \cdot (-\boldsymbol{v}_{\mathrm{NEA}})$!

Two different targeting options can be conceived. The first one is a collision trajectory that maximizes the head-on impact velocity, the second one is an exactly retrograde orbit (ERO), where the solar sail KEI encounters the target at every perihelion and aphelion passage. The resulting deflections achieved with the different strategies, as well as the parabolic limit case (spacecraft is on a parabolic trajectory), are shown in Table 1 for different pre-2029 impact dates.

Table 1. Pre-2029-encounter impacts

Impact Date	MJD	Days before 2029-encounter	KEI head-on impact velocity [km/s]	Worst case velocity change from a single KEI [mm/s]	Deflection from a single KEI estimated [km]	Deflection from a single KEI calculated [km]	Fig.
From trajectory that maximizes the impact velocity:							
02 Jan 2026	61042.4	1198.0	75.38	0.2811	87.3	93.2	7(a)
22 Nov 2026	61366.0	874.4	77.91	0.2905	65.8	71.6	
11 Oct 2027	61689.6	550.8	80.28	0.2993	42.7	48.7	
30 Aug 2028	62013.2	227.2	80.95	0.3018	17.8	23.3	
From exactly retrograde orbit:							
02 Jan 2026	61042.4	1198.0	75.26	0.2806	87.1	93.2	7(b)
22 Nov 2026	61366.0	874.4	75.26	0.2806	63.6	69.5	
11 Oct 2027	61689.6	550.8	75.26	0.2806	40.1	45.8	
30 Aug 2028	62013.2	227.2	75.26	0.2806	16.5	21.9	
Parabolic limit case:							
02 Jan 2026	61042.4	1198.0	86.39	0.3221	100.0	107.0	
22 Nov 2026	61366.0	874.4	86.39	0.3221	73.0	79.8	
11 Oct 2027	61689.6	550.8	86.39	0.3221	46.0	52.5	
30 Aug 2028	62013.2	227.2	86.39	0.3221	19.0	25.1	

The effectiveness of both options can be assessed by comparing the impact velocities with the maximum possible impact velocity that results from the parabolic limit case. The third column in Table 1 shows the lead time Δt_{L} before the 2029-encounter, the fourth column shows the impact velocity v_{imp}, the fifth column shows the resulting velocity change Δv of the asteroid, as calculated from Eq. (2), and the sixth column shows the deflection, as calculated from Eq. (1). The seventh column shows the deflection, as calculated by numerical integration.

For trajectories that maximize the impact velocity, Table 1 shows how v_{imp} increases for later impact dates. This, however, is over-compensated by the shorter lead times before the 2029-encounter, so that the earliest possible impact yields the largest 2029-deflection and is therefore preferable. The earliest possible impact opportunity is 02 Jan 2026 because for the earlier perihelion passage on 12 Feb 2025, the available Δt_{trg} is not sufficient to reach the asteroid. The targeting trajectory that maximizes the impact velocity for this date is shown in Fig. 7(a).

If the impact does not take place on 02 Jan 2026 but is turned into a flyby (by intention or accidence), the next impact opportunity is 11 Oct 2027. An impact on 22 Nov 2026 is not possible because a 1:1 resonant trajectory cannot be achieved in this short time.

The second targeting option impacts Apophis from an exactly retrograde orbit. Being in a 1:1 resonance (at least when the sail is jettisoned or oriented perpendicular to the sun), the solar sail KEI encounters the target at every perihelion and aphelion passage. Consequently, v_{imp} does not change for the different perihelion impact opportunities. The trajectory to achieve such an ERO is shown in Fig. 7(b). Because this orbit is already attained on 26 Dec 2025, it can also impact Apophis on 02 Jan 2026. The v_{imp} for the first option is only 0.16% higher. Also for later impacts, the slightly lower achievable impact velocities from an ERO are compensated by the flexibility in choosing the impact date, which is only given by this option.

If not a single KEI but more KEIs are used to impact on Apophis before its 2029-encounter, it could be nudged farther out of the keyhole but unfortunately not out of the geostationary orbit because this would

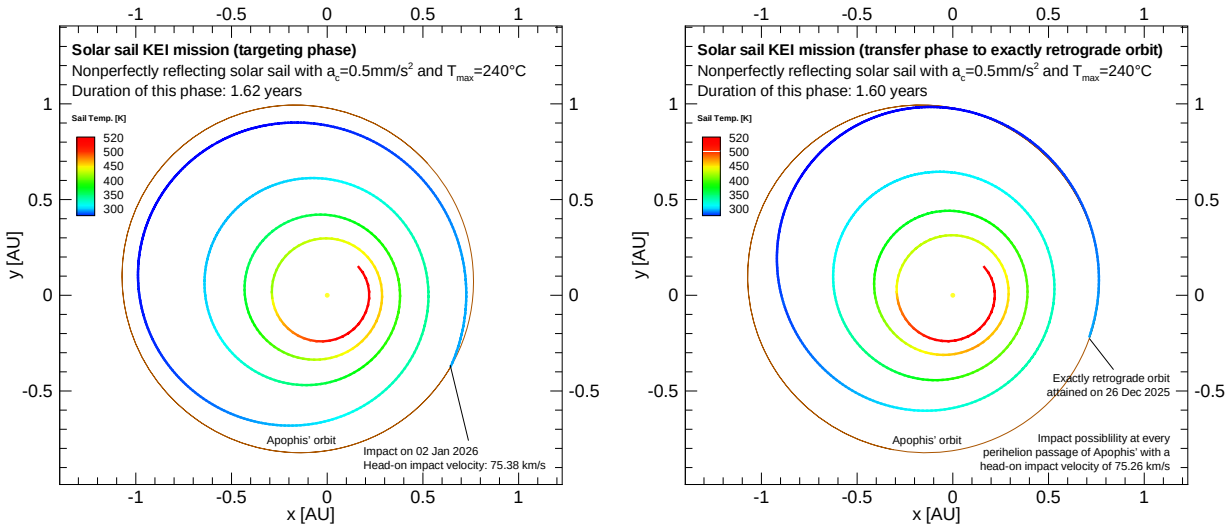

(a) Trajectory that maximizes the impact velocity

(b) Transfer trajectory to exactly retrograde orbit

Figure 7. Targeting trajectories for an impact on 02 Jan 2026

only be possible with a prograde impact. This is because a retrograde KEI impact decreases Apophis' orbital energy and thus decreases Apophis' orbital period so that it will arrive earlier at the "impact point", so that the trailing-side flyby distance will become reduced. This way, every retrograde impact moves the closest encounter about 90 km closer to Earth. Because a single KEI might fail to hit the target, however, the use of more KEIs adds redundancy and is thus advisable.

D. Targeting Trajectory Optimization for the Post-2029-Encounter Impact

In Ref. 38, Kahle has generated 20 000 potential Apophis orbits by random variation of the orbital elements within the 3σ-accuracy. Two of them (here termed Ap1 and Ap2) have been found to collide with the Earth, both during a 7:6 resonant return on 13 Apr 2036. They are used as potential impact-trajectories within this paper. Their orbital elements, before and after the 2029-encounter, are listed in Table 2, and their impacting orbits are shown in Fig. 8. Figure 8(a) shows a graphical comparison of Ap1's and Ap2's pre- and post-2029-encounter orbit (the orbits are so similar that they are not distinguishable in plot 8(a)).

Table 2. Orbital elements of the Earth-impacting Apophis orbit variations Ap1 and Ap2

	before 2029-encounter		after 2029-encounter	
	Ap1	Ap2	Ap1	Ap2
MJD	53459.0	53459.0	64699.0	64699.0
a[AU]	0.9223913	0.9223912	1.1082428	1.1082581
e	0.191038	0.191038	0.190763	0.190753
i[deg]	3.331	3.331	2.166	2.169
ω[deg]	126.384	126.383	70.230	70.227
Ω[deg]	204.472	204.472	203.523	203.523
M[deg]	203.974	203.974	227.857	227.854

Two different targeting options are considered. The first one is a collision trajectory that maximizes right after launch the head-on impact velocity for an impact on the earliest possible post-2029-encounter impact date, 11 Jun 2029, shortly after the 2029-encounter (Fig. 9). The second one is from the previous pre-2029-encounter impact trajectory that was turned into a flyby on 02 Jan 26 and is now also determined for an impact with maximum head-on velocity on 11 Jun 2029 (Fig.10). The resulting deflections achieved

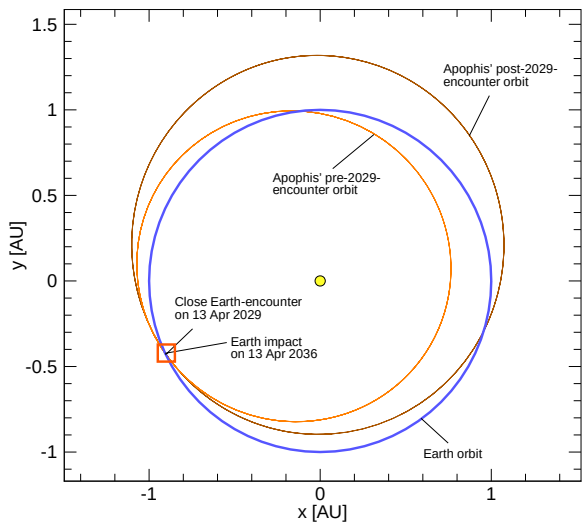

(a) Comparison of Ap1's pre- and post-2029-encounter orbit

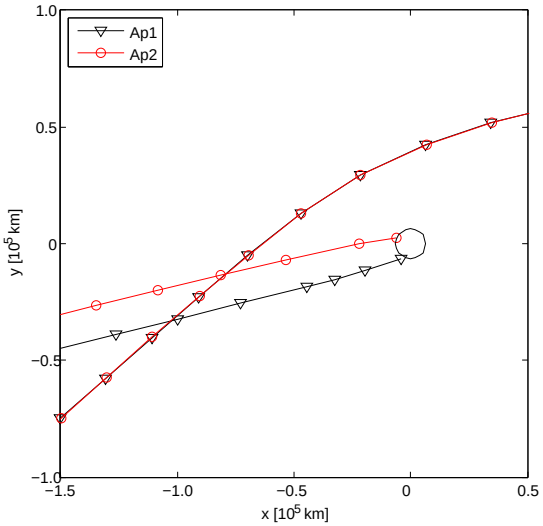

(b) Closeup of the 2029-encounter and the impact (geocentric reference frame)

Figure 8. Earth-impacting Apophis variations

with the different strategies, as well as the parabolic limit case, are shown in Table 3 for two different post-2029-encounter impact dates.

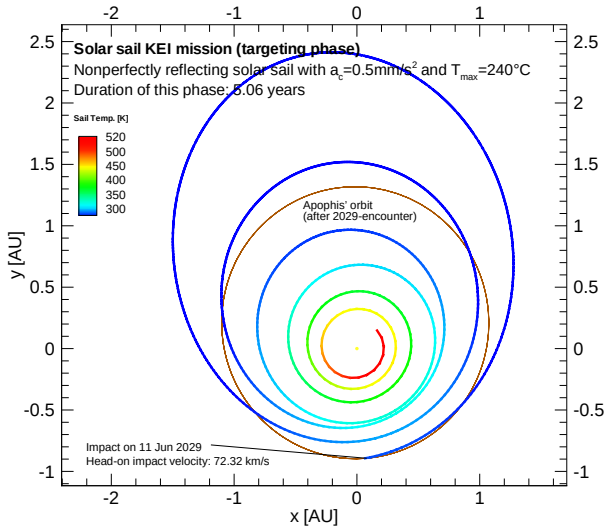

(a) Impact from trajectory that maximizes the impact velocity

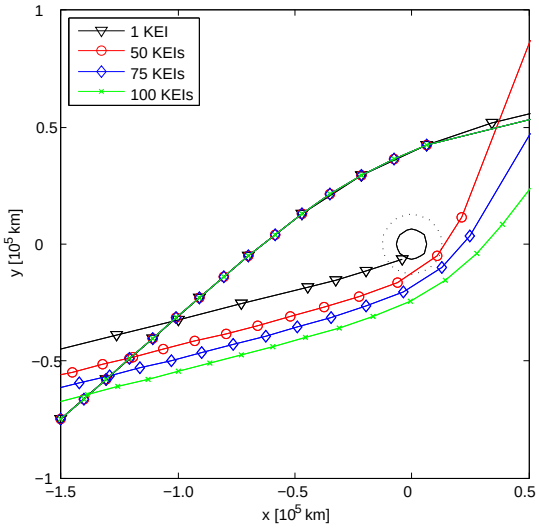

(b) Deflection for different numbers of KEIs (Ap1, geocentric reference frame)

Figure 9. Targeting trajectory for an impact on 11 Jun 2029

The effectiveness of both options can be assessed by comparing the impact velocities with the maximum possible impact velocity that results from the parabolic limit case. Again, v_{imp} increases for the later impact date, but is over-compensated by the shorter lead time before the 2036-impact, so that the earliest possible impact yields the largest 2036-deflection and is therefore preferable. Note that the deviations between the estimated and the numerically calculated deflections in Table 3 result from the simplifying assumptions that underly Eq. (1) (e.g. the neglect of Earth's gravitational field).

Figure 11 shows the Δv that is required for a successful deflection of Ap1 and Ap2 to a safe distance of 2 Earth radii, as well as the optimal deflection angles according to the analysis performed in Ref. 38.

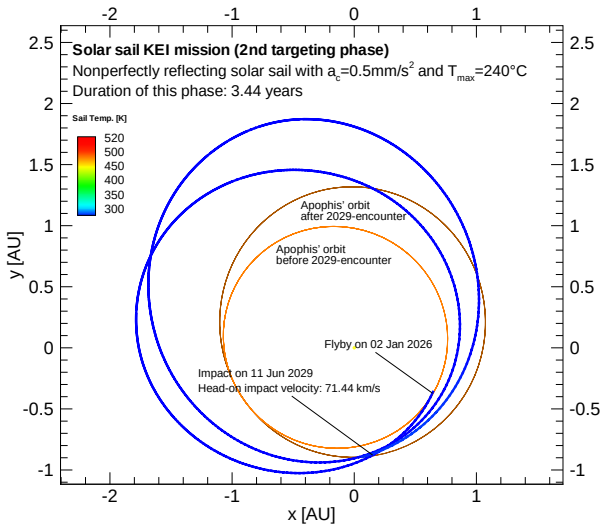

Figure 10. Targeting trajectory for an impact on 11 Jun 2029 (impact from a pre-2029-encounter impact trajectory, i.e. 02 Jan 2026 flyby)

Table 3. Post-2029-encounter impacts

Impact Date	MJD	Days before 2036-impact	KEI head-on impact velocity [km/s]	Worst case velocity change from a single KEI [mm/s]	Deflection from a single KEI estimated [km]	Deflection from a single KEI calculated [km]	Fig.
From trajectory that maximizes the impact velocity:							
11 Jun 2029	62298.6	2498.9	72.32	0.2697	174.7	104.0	9
11 Aug 2030	62724.7	2072.8	74.11	0.2763	148.5	25.8-74.3	
From pre-2029-encounter impact trajectory (02 Jan 26 flyby):							
11 Jun 2029	62298.6	2498.9	71.44	0.2664	172.5	102.1	10
Parabolic limit case:							
11 Jun 2029	62298.6	2498.9	78.80	0.2938	190.3	114.1	
11 Aug 2030	62724.7	2072.8	78.80	0.2938	157.9	26.7-81.2	

One can see that after the 2029-encounter a successful deflection of Apophis requires in the best case less than about 100 KEIs, assuming that every consecutive KEI impact has the optimal deflection angle and provides the same Δv of 0.2697 mm/s, which might not be possible for a "rubble-pile". Numerical integration shows that 70-75 KEIs are required for a successful deflection of Ap1. For Ap2, the situation is worse because the optimal post-2029-deflection requires a prograde impact (which is not possible with very high impact velocities), as can be seen from Ap2's optimal deflection angle in the lower diagram, so that the deflection has to "cross" the Earth. Numerical integration shows that in this case 130-140 KEIs are required. Because it is not known before whether the real Apophis-orbit would be like Ap1 or like Ap2, a worst case scenario should be assumed, which might require about 200 KEIs (also taking into account that some KEIs might miss the target). Even if the asteroid fragments, the largest fragments could be crushed. The interplanetary insertion mass for 200 KEIs is 63.2 mt. This would require 7 Delta IV Heavy (9.3 mt to $C_3 = 0\,\mathrm{km}^2/\mathrm{s}^2$, Ref. 39), 10 Atlas 5 (6.5 mt to $C_3 = 0\,\mathrm{km}^2/\mathrm{s}^2$, Ref. 39), or 6 Ariane 5 ESC-B (10.8 mt to $C_3 = 0\,\mathrm{km}^2/\mathrm{s}^2$, Ref. 40). In comparison to the catastrophic results of an impact, this is very feasible. Of course a pre-encounter impact is clearly the better option for Apophis, but this option might not be available for other NEOs that do not have a close encounter before they impact the Earth.

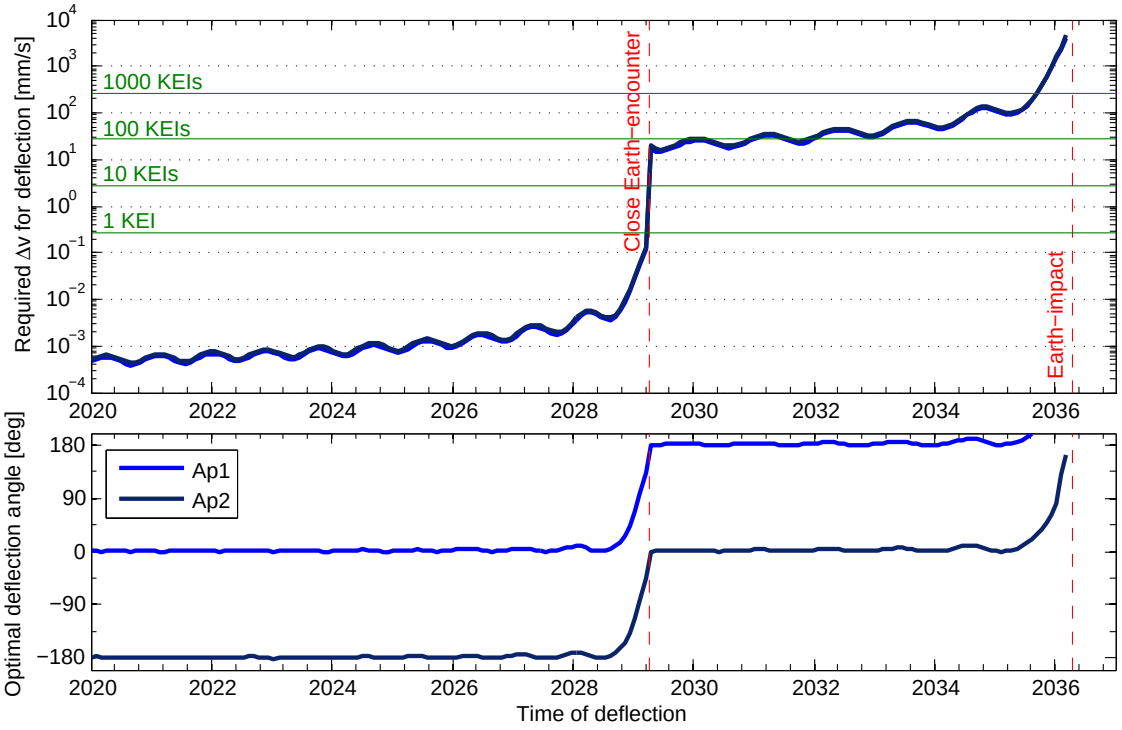

Figure 11. Required velocity change and optimal deflection angle for Ap1 and Ap2

VIII. Variation of Mission Design Parameters

A. Variation of the Hyperbolic Excess Energy for Interplanetary Insertion

The influence of the hyperbolic excess energy for interplanetary insertion, C_3, on the mission performance of solar sail KEI missions was investigated in Ref. 14. Those results are transferable to the Apophis mission and are therefore not repeated here. Of course a larger C_3 shortens the time that is required for orbit cranking and therefore extends the time available for the targeting phase, allowing, e.g., a later launch, a more massive impactor (lower a_c), or a larger impact velocity.

B. Variation of the Sail Temperature Limit

In this section, the influence of the solar sail temperature limit T_{lim} on the mission performance of solar sail KEI missions is investigated. Figure 12 shows for a circular orbit, how the inclination change rate varies with the orbit-cranking semi-major axis for different solar sail temperature limits, i.e. $(\Delta i/\Delta t)(T_{\mathrm{lim}}, a_{\mathrm{cr}})$. For $220°\mathrm{C} \leq T_{\mathrm{lim}} \leq 260°\mathrm{C}$, the optimal orbit-cranking semi-major axis can be approximated with an error of less than 2% by

$$\widetilde{a}_{\mathrm{cr,opt}} \approx 1.4805 - 0.23 \cdot \ln(\widetilde{T}_{\mathrm{lim}}) \tag{13}$$

where $\widetilde{a}_{\mathrm{cr,opt}} = \frac{a_{\mathrm{cr,opt}}}{1\,\mathrm{AU}}$ and $\widetilde{T}_{\mathrm{lim}} = \frac{T_{\mathrm{lim}}}{1°\mathrm{C}}$. The maximum inclination change rate can be approximated with an error of less than 1% by

$$\widetilde{(\Delta i/\Delta t)}_{\max} \approx 0.0224 \cdot \widetilde{a}_{\mathrm{cr,opt}}^{-1.32} \tag{14}$$

where $\widetilde{(\Delta i/\Delta t)}_{\max} = \frac{(\Delta i/\Delta t)_{\max}}{1\,\mathrm{deg/day}}$.

We used InTrance to optimize the orbit-cranking phase for different solar sail temperature limits ($220°\mathrm{C} \leq T_{\mathrm{lim}} \leq 260°\mathrm{C}$). The results are shown in Table 4 and Fig. 13. Figure 13(b) shows that InTrance matches the optimal orbit-cranking semi-major axes shown in Fig. 12 very closely. For $220°\mathrm{C} \leq T_{\mathrm{lim}} \leq 260°\mathrm{C}$, the time required for the orbit-cranking phase can be approximated with an error of less than 1% by

$$\widetilde{\Delta t}_{\mathrm{oc}} \approx 765(1 - \widetilde{a}_{\mathrm{cr,opt}}) + \frac{166.7}{\widetilde{(\Delta i/\Delta t)}_{\max}} \tag{15}$$

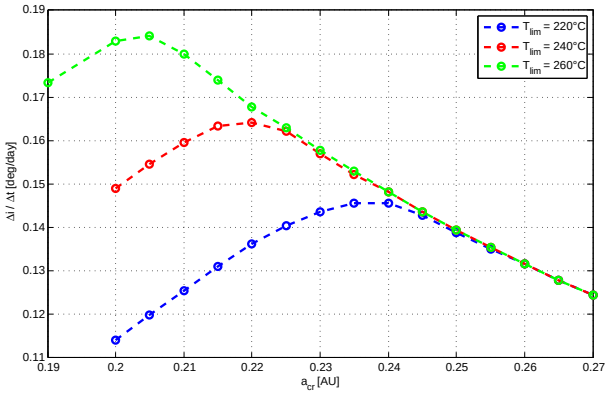

Figure 12. Inclination change rate over orbit-cranking semi-major axis for different solar sail temperature limits, circular orbit

Note that in Eq. (19) 166.7 is the required inclination change in degrees and $1 - \widetilde{a}_{\mathrm{cr,opt}}$ is the spiralling-in distance in astronomical units.

Table 4. Variation of T_{lim}

T_{lim} [°C]	$a_{\mathrm{cr,opt}}$ [AU]	$(\Delta i/\Delta t)_{\max}$ [deg/day]	Δt_{oc} [days]
220	0.236	0.1461	1722
240	0.220	0.1648	1604
260	0.205	0.1838	1513

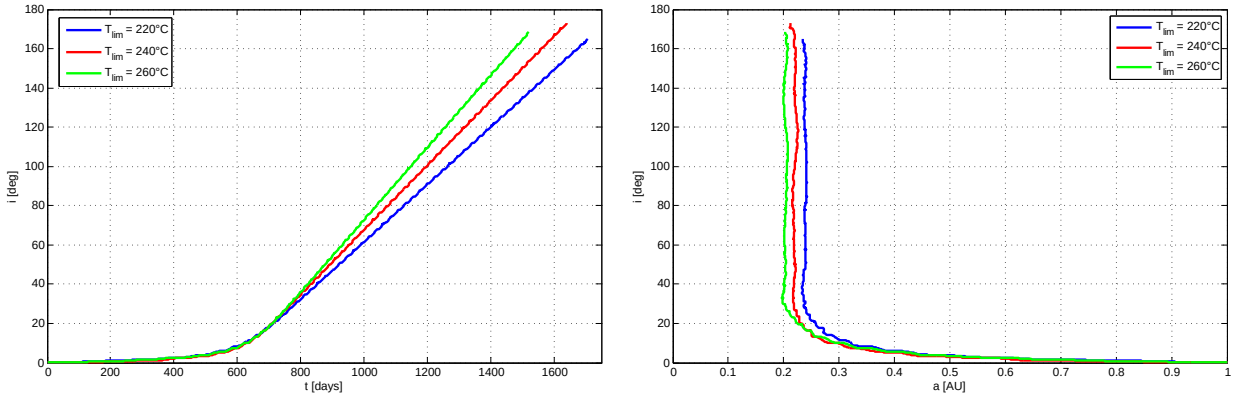

(a) inclination over flight time, $i(t)$

(b) inclination over semi-major axis, $i(a)$

Figure 13. Orbit-cranking phase: variation of T_{lim}

IX. Solar Sail Degradation

To investigate the effects of optical degradation of the sail film, as it is expected in the extreme space environment close to the sun, we apply here the parametric model developed in Ref. 41. In this parametric model the optical parameters p are assumed to depend on the cumulated solar radiation dose (SRD) $\Sigma(t)$

on the sail:

$$\frac{p(t)}{p_0} = \begin{cases} \left(1 + d\mathrm{e}^{-\lambda\Sigma(t)}\right) / (1+d) & \text{for} \quad p \in \{\rho, s\} \\ 1 + d\left(1 - \mathrm{e}^{-\lambda\Sigma(t)}\right) & \text{for} \quad p = \varepsilon_\mathrm{f} \\ 1 & \text{for} \quad p \in \{\varepsilon_\mathrm{b}, B_\mathrm{f}, B_\mathrm{b}\} \end{cases} \tag{16}$$

The (dimensionless) SRD is

$$\Sigma(t) = \frac{\tilde{\Sigma}(t)}{\tilde{\Sigma}_0} = \left(r_0^2 \int_{t_0}^{t} \frac{\cos\alpha}{r^2}\, dt' \right) \Big/ 1\,\mathrm{yr} \tag{17}$$

with $\tilde{\Sigma}_0 \triangleq S_0 \cdot 1\,\mathrm{yr} = 1368\,\mathrm{W/m^2} \cdot 1\,\mathrm{yr} = 15.768\,\mathrm{TJ/m^2}$ being the annual SRD on a surface perpendicular to the sun at 1 AU. The degradation constant λ is related to the "half life solar radiation dose" $\hat{\Sigma}$ ($\Sigma = \hat{\Sigma} \Rightarrow p = \frac{p_0 + p_\infty}{2}$) via

$$\lambda = \frac{\ln 2}{\hat{\Sigma}} \tag{18}$$

The degradation factor d defines the end-of-life values p_∞ of the optical parameters:

$$\rho_\infty = \frac{\rho_0}{1+d} \qquad s_\infty = \frac{s_0}{1+d} \qquad \varepsilon_{\mathrm{f}\infty} = (1+d)\varepsilon_{\mathrm{f}0}$$
$$\varepsilon_{\mathrm{b}\infty} = \varepsilon_{\mathrm{b}0} \qquad B_{\mathrm{f}\infty} = B_{\mathrm{f}0} \qquad B_{\mathrm{b}\infty} = B_{\mathrm{b}0}$$

Figure 14 and Table 5 show the results for different degradation factors $0 \le d \le 0.2$, assuming a half life SRD of $25\,S_0 \cdot 1\,\mathrm{yr} = 394\,\mathrm{TJ/m^2}$.

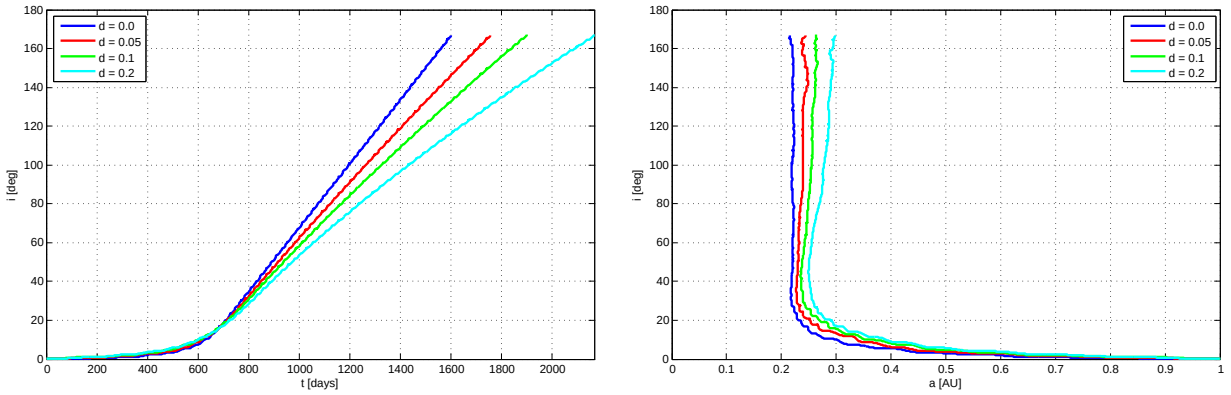

(a) inclination over flight time, $i(t)$

(b) inclination over semi-major axis, $i(a)$

Figure 14. Orbit-cranking phase: different degradation factors ($T_\mathrm{lim} = 240°\mathrm{C}$)

Table 5. Attainment of an exactly retrograde orbit (ERO) with degradation

Degradation factor	Δt_oc [days]	Transfer time to ERO (Δt) [days]	Attainment of ERO		Earliest possible Apophis impact		Calculated deflection from a single KEI [km]
			MJD	Date	MJD	Date	
0.0	1601	2186	61035	26 Dec 2025	61042.4	02 Jan 2026	93.2
0.05	1756	2395	61244	23 Jul 2026	61366.0	22 Nov 2026	69.5
0.1	1897	2574	61423	18 Jan 2027	61689.6	11 Oct 2027	45.8
0.2	2166	2816	61665	17 Sep 2027	61689.6	11 Oct 2027	45.8

For $0 \le d \le 0.2$, the time required for the orbit-cranking phase can be approximated with an error of less than 0.5% by

$$\widetilde{\Delta t}_\mathrm{oc} \approx 1609 + 2809 \cdot d \tag{19}$$

Such a simple approximation is not possible for the time that is required to attain the ERO because of the required correct phasing of the ERO with Apophis' orbit.

It can be seen from Table 5 that already for a small degradation of $d = 0.05$ it is not possible anymore to impact the asteroid on the intended perihelion passage on 02 Jan 2026 but one passage later on 22 Nov 2026. Consequently, the deflection is much smaller, 69.5 km instead of 93.2 km. However, even for a larger degradation of $d = 0.2$, it is still possible to prevent Apophis from flying through a keyhole. Figure 14(b) shows that for larger degradation factors it is favorable to crank the orbit further away from the sun than it would be optimal without degradation. The main degradation effect can be seen from Fig. 14(a), which shows that $\Delta i/\Delta t$ becomes smaller with increasing SRD. Because optical degradation is an important factor for this mission, and because the real degradation behavior of solar sails in the space environment is to a considerable degree unknown, extensive ground and in-space tests are required prior to this mission.

X. Conclusions

We have shown that solar sails are a realistic option to deflect asteroid 99942 Apophis with a kinetic impact from a retrograde orbit. For a launch at the beginning of 2020, we have considered two basically different scenarios. For both scenarios, we have used a 160 m × 160 m, 168 kg solar sail to bring a separable 150 kg kinetic energy impactor (KEI) onto a collision course with the asteroid. In the first scenario, a single KEI is used to impact Apophis before its close Earth-encounter in 2029, thus being able to nudge it out of a gravitational keyhole that would lead to a resonant return in 2036. An exactly retrograde orbit, where the KEI can impact the asteroid at every perihelion (and aphelion) passage, is the most flexible option for this scenario. In the second scenario, an impact after Apophis' close encounter in 2029 was considered. We have found that in this case many KEIs (up to 200, depending sensitively on the actual impact trajectory) would be necessary to prevent Apophis from impacting the Earth. Nevertheless, requiring less than 10 heavy lift launch vehicles, this option is still feasible. Of course a pre-encounter impact is clearly the better option for Apophis, but this option might not be available for other NEOs that do not have a close encounter before they impact the Earth.

We have also found that the mission performance might be seriously affected by optical degradation of the sail surface, as it is expected in the extreme space environment close to the sun. Because the real degradation behavior of solar sails in the space environment is to a considerable degree unknown, ground and in-space tests are required prior to this mission. The required solar sail technology for such a mission, however, is not yet state-of-the-art, but would have to be developed in a sharply pursued technological program within the next 10 to 20 years. Other problems that have to be considered for the design of this mission are the extreme requirements for the terminal guidance prior to impact (accuracy much better than 100 m at a relative velocity of more than 75 km/s) and the thermal control that has to make the spacecraft withstand very close solar distances ($0.2 - 0.25$ AU).

Acknowledgements

The work described in this paper was funded in part by the In-Space Propulsion Technology Program, which is managed by NASA's Science Mission Directorate in Washington, D.C., and implemented by the In-Space Propulsion Technology Office at Marshall Space Flight Center in Huntsville, Alabama. The program objective is to develop in-space propulsion technologies that can enable or benefit near and mid-term NASA space science missions by significantly reducing cost, mass or travel times.

References

[1]European Asteroid Research Node Website, http://earn.dlr.de.

[2]Commitee on Planetary and Lunar Exploration, Space Studies Board, and Commission on Physical Sciences, Mathematics, and Applications, "The Exploration of Near-Earth Objects," Tech. rep., National Research Council, 1998.

[3]Rampino, M. and Haggerty, B., "Extraterrestrial Impacts and Mass Extinctions of Life," *Hazards Due to Comets and Asteroids*, edited by T. Gehrels, The University of Arizona Press, Tucson, USA, 1994, pp. 827–857.

[4]Ward, P. and Brownlee, D., *Rare Earth. Why Complex Life Is Uncommon in the Universe*, Copernicus, New York, 2000.

[5]Morrison, D., Chapman, C., and Slovic, P., "The Impact Hazard," *Hazards Due to Comets and Asteroids*, edited by T. Gehrels, The University of Arizona Press, Tucson, USA, 1994, pp. 59–91.

[6]Hills, J., Nemchinov, I., Popov, S., and Teterev, A., "Tsunami Generated by Small Asteroid Impacts," *Hazards Due to*

Comets and Asteroids, edited by T. Gehrels, The University of Arizona Press, Tucson, USA, 1994, pp. 779–789.

[7]Bottke, W., Nolan, M., Greenberg, R., and Kolvoord, R., "Collisional Lifetimes and Impact Statistics of Near-Earth Asteroids," *Hazards Due to Comets and Asteroids*, edited by T. Gehrels, The University of Arizona Press, Tucson, USA, 1994, pp. 337–357.

[8]Gladman, B., Michel, P., and Froeschle, C., "The Near-Earth Object Population," *Icarus*, Vol. 146, 2000, pp. 176–189.

[9]de Pater, I. and Lissauer, J., *Planetary Sciences*, Cambridge University Press, Cambridge, New York, Melbourne, 2001.

[10]McInnes, C., "Deflection of Near-Earth Asteroids by Kinetic Energy Impacts From Retrograde Orbits," *Planetary and Space Science*, Vol. 52, 2004, pp. 587–590.

[11]McInnes, C., Hughes, G., and Macdonald, M., "High-Energy Small Body Missions Using Solar Sail Propulsion," 56$^{\text{th}}$ International Astronautical Congress, Fukuoka, Japan, October 2005, IAC-05-A3.5.B.

[12]Wie, B., "Solar Sailing Kinetic Energy Interceptor (KEI) Mission for Impacting/Deflecting Near-Earth Asteroids," 41$^{\text{st}}$ AIAA/ASME/SAE/ASEE Joint Propulsion Conference and Exhibit, Tucson, USA, July 2005, AIAA Paper 2005-3725.

[13]Wie, B., "Solar Sailing Kinetic Energy Interceptor (KEI) Mission for Impacting and Deflecting Near-Earth Asteroids," AIAA Guidance, Navigation, and Control Conference, San Francisco, USA, August 2005, AIAA Paper 2005-6175.

[14]Dachwald, B. and Wie, B., "Solar Sail Trajectory Optimization for Intercepting, Impacting, and Deflecting Near-Earth Asteroids," AIAA Guidance, Navigation, and Control Conference, San Francisco, USA, August 2005, AIAA Paper 2005-6176, also submitted to the Journal of Spacecraft and Rockets.

[15]Wright, J., "Solar Sailing – Evaluation of Concept and Potential," Tech. rep., Battelle Columbus Laboratories, Columbus, Ohio, March 1976, BMI-NLVP-TM-74-3.

[16]Wright, J. and Warmke, J., "Solar Sail Mission Applications," AIAA/AAS Astrodynamics Conference, San Diego, USA, August 18-20, 1976, AIAA Paper 76-808.

[17]Sauer, C., "A Comparison of Solar Sail and Ion Drive Trajectories for a Halley's Comet Rendezvous Mission," AAS/AIAA Astrodynamics Conference, Jackson, USA, September 1977, AAS Paper 77-104.

[18]Near Earth Objects Dynamic Site Website, http://newton.dm.unipi.it/cgi-bin/neodys/ neoibo.

[19]NASA's Near-Earth Object Program Website, http://neo.jpl.nasa.gov.

[20]Chesley, S., "Potential Impact Detection for Near-Earth Asteroids: The Case of 99942 Apophis (2004 MN4)," *Asteroids, Comets, Meteors. Proceedings IAU Symposium No. 229*, edited by S. Ferraz-Mello and D. Lazzaro, Cambridge University Press, Cambridge, New York, Melbourne, 2006.

[21]Gehrels, T., editor, *Deflection and Fragmentation of Near-Earth Asteroids*. The University of Arizona Press, Tucson, USA, 1994.

[22]Holsapple, K., "About Deflecting Asteroids and Comets," *Mitigation of Hazardous Comets and Asteroids*, edited by M. Belton, T. Morgan, N. Samarasinha, and D. Yeomans, Cambridge University Press, Cambridge, New York, Melbourne, 2004, pp. 113–140.

[23]Fujiwara, A., Kawaguchi, J., Yeomans, D., Abe, M., Mukai, T., Okada, T., Saito, J., Yano, H., Yoshikawa, M., Scheeres, D., Barnouin-Iha, O., Cheng, A., Demura, H., Gaskell, R., Hirata, N., Ikeda, H., Kominato, T., Miyamoto, H., Nakamura, A., Nakamura, R., Sasaki, S., and Uesugi, K., "The Rubble-Pile Asteroid Itokawa as Observed by Hayabusa," *Science*, Vol. 312, 2006, pp. 1330–1334.

[24]Housen, R. and Holsapple, K., "Impact Cratering on Porous Asteroids," *Icarus*, Vol. 163, 203, pp. 102–119.

[25]Holsapple, K., Giblin, I., Housen, K., Nakamura, A., and Ryan, E., "Asteroid Impacts: Laboratory Experiments and Scaling Laws," *Asteroids III*, edited by W. Bottke, A. Cellino, and P. Paolicchi, Space Science Series, University of Arizona Press, Tucson, 2002, pp. 443–462.

[26]Shafer, B., Garcia, M., Scammon, R., Snell, C., Stellingwerf, R., Remo, J., Managan, R., and Rosenkilde, C., "The Coupling of Energy to Asteroids and Comets," *Hazards Due to Comets and Asteroids*, edited by T. Gehrels, The University of Arizona Press, Tucson, USA, 1994, pp. 955–1012.

[27]Blume, W., "Deep Impact: Mission Design Approach for a New Discovery Mission," *Acta Astronautica*, Vol. 52, No. 2-6, 2003, pp. 105–110.

[28]NASA's Deep Impact Mission Web Site, http://deepimpact.jpl.nasa.gov.

[29]ESA's Don Quijote Mission Web Site, http://www.esa.int/gsp/NEO/quijote/quijote.htm.

[30]Wright, J., *Space Sailing*, Gordon and Breach Science Publishers, Philadelphia, 1992.

[31]McInnes, C., *Solar Sailing. Technology, Dynamics and Mission Applications*, Springer–Praxis Series in Space Science and Technology, Springer–Praxis, Berlin, Heidelberg, New York, Chicester, 1999.

[32]Garbe, G., Wie, B., Murphy, D., Ewing, A., Lichodziejewski, L., Derbes, B., Campbell, B., Wang, J., Taleghani, B., Canfield, S., Beard, J., and Peddieson, J., "Solar Sail Propulsion Technology Development," *Recent Advances in Gossamer Spacecraft*, edited by C. Jenkins, Vol. 212 of *Progress in Astronautics and Aeronautics*, American Institute of Aeronautics and Astronautics, Reston, 2006, pp. 191–261.

[33]Battin, R., *An Introduction to the Mathematics and Methods of Astrodynamics*, AIAA Education Series, American Institute of Aeronautics and Astronautics, Reston, revised ed., 1999.

[34]Dachwald, B., *Low-Thrust Trajectory Optimization and Interplanetary Mission Analysis Using Evolutionary Neurocontrol*, Doctoral thesis, Universität der Bundeswehr München; Fakultät für Luft- und Raumfahrttechnik, 2004.

[35]Dachwald, B., "Optimization of Interplanetary Solar Sailcraft Trajectories Using Evolutionary Neurocontrol," *Journal of Guidance, Control, and Dynamics*, Vol. 27, No. 1, pp. 66–72.

[36]Dachwald, B., "Optimization of Very-Low-Thrust Trajectories Using Evolutionary Neurocontrol," *Acta Astronautica*, Vol. 57, No. 2-8, 2005, pp. 175–185.

[37]Dachwald, B., "Optimal Solar Sail Trajectories for Missions to the Outer Solar System," *Journal of Guidance, Control, and Dynamics*, Vol. 28, No. 6, 2005, pp. 1187–1193.

[38]Kahle, R., Hahn, G., and Kührt, E., "Optimal Deflection of NEOs en Route of Collision with the Earth," *Icarus*, Vol. 182, 2006, pp. 482–488.

[39]Isakowitz, S., Hopkins, J., and Hopkins Jr., J., *International Reference Guide to Space Launch Systems*, American Institute of Aeronautics and Astronautics, Reston, 4th ed., 2004.

[40]Ancarola, B., "Ariane 5 Performance Optimisation for Interplanetary Missions," AIAA/AAS Astrodynamics Specialist Conference, Monterey, USA, August 2002, AIAA Paper 2002-4902.

[41]Dachwald, B., Mengali, G., Quarta, A., and Macdonald, M., "Parametric Model and Optimal Control of Solar Sails with Optical Degradation," *Journal of Guidance, Control, and Dynamics*, accepted.